AD/SSC/Tech. No. 88

Accelerator Development Department

BROOKHAVEN NATIONAL LABORATORY

Associated Universities, Inc.

Upton, New York 11973

SSC Technical Note No. 88

SSCL-N-699

DSX201/W6733 - COIL AND IRON DESIGN FOR SSC 50 mm DIPOLE MAGNET WITH WIDER CABLES

R. C. Gupta, S. A. Kahn and G. H. Morgan

June 28, 1990

DSX201/W6733 - Coil and Iron Design for SSC 50 mm Dipole Magnet with Wider Cables

R.C. Gupta, S.A. Kahn and G.H. Morgan

28 June 1990

1. Introduction

In this note we shall present the optimized design of the two dimensional coil and iron cross section for the SSC dipole magnet with 50 mm coil i.d. and with wider cables; the cable used in the inner layer has 30 strands and in the outer 36. The magnet is expected to have a margin of more than 12% over the design central field value of 6.6 Tesla for the copper to superconductor ratio of 1.3* in the cable used in the inner layer and of 1.8 in the cable used in the outer layer. The computed maximum change in the sextupole harmonic, b_2', due to iron saturation is about 0.3 prime unit. The variation in field harmonics as a function of central field, as calculated by the computer codes POISSON, MDP and PE2D, will be presented here. The quench performance predictions, the stored energy calculations, the effect of random errors on the coil placement and the computed value of the Lorentz forces on the coil will also be presented. The coil cross section is specified in BNL drawing number 22.00-561-3** and the iron in drawing No. 22-00.563-4.

2. Coil Design

In section 2.1 we shall describe the general considerations and criteria used in selecting a particular coil configuration. This final design will be discussed in more detail in section 2.2. The field harmonics will be discussed in section 2.3.

---

* The copper to superconductor ratio has been revised to 1.5 in the cable used in the inner layer to reduce the current density in the copper; this reduces the field margin to 10.2% in the inner layer.

** We have done the computations and design assuming the width of the cable used in the inner layer being 0.477″. However, this width has been revised to 0.486″. The effects of this change will be reported in a subsequent note.

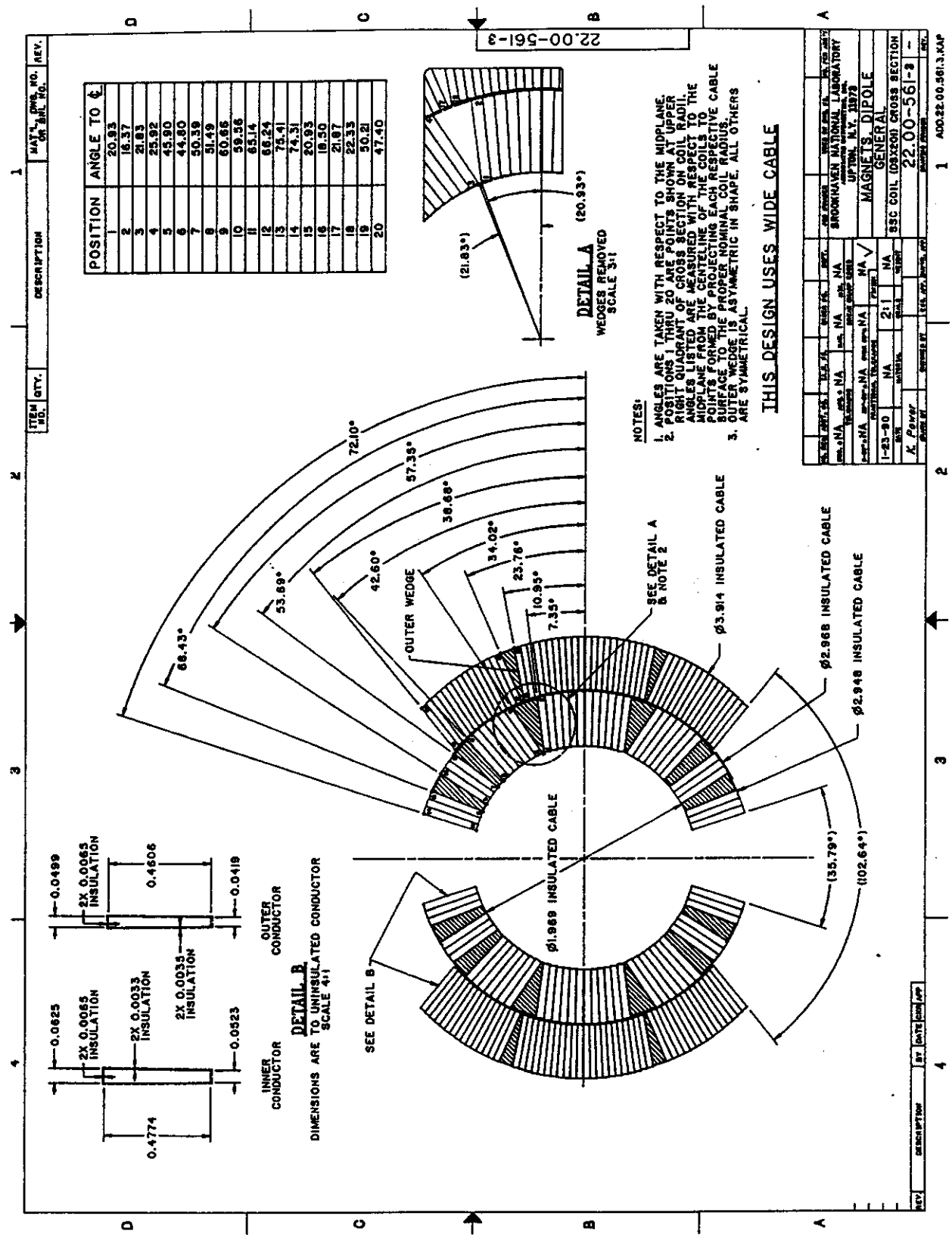

Figure 2.1: Optimized Coil for DSX201/W6733.

Table 2.3: Details of the wedges. Inner layer has three wedges and outer has one.

Wedge No.	1	2	3	4
Insulated width, mm	12.12	12.40	12.40	11.95
Minimum thickness				
Insulated, degree	1.413	4.542	4.542	1.053
Insulated, mil	21.9	77.4	77.4	27.3
Bare, mil	15.3	70.8	70.8	20.4
Insulated mid thickness				
In mm	135	125	125	79
In mil	3.43	3.17	3.17	2.01
Insulated angle, deg	26.66	11.09	11.09	12.82
Face angles				
CW(Bottom)	-10.76	-2.64	-2.64	-8.57
CCW(Top)	9.68	2.64	2.64	1.63

to the line joining the midpoints of its inner and outer radial surfaces. In this case the two face angles of this wedge are equal in magnitude and opposite in sign. These features reduce the chance of errors or mix-ups during magnet construction. We will discuss below how it was done using the computer program PAR2DOPT.

The way the coil configuration is constructed in PAR2DOPT the wedge between block No. 3 and block No. 4 (wedge No. 3) is naturally symmetric because these two blocks have the same number of turns (three) in them and they are radial (no tilt). We imposed a condition that wedge No 2 and wedge No. 3 have the same size in degrees (at the inner radius of the wedge as measured from the center of the dipole). We also introduced a pre-computed tilt of $-4.35°$ in block No. 2 (see Table 2.2) which makes the CW side (bottom side) of wedge No. 2 same as that of wedge No. 3. These conditions make wedge No. 2 and 3 both same and symmetric (see Table 2.3). In addition the wedge No. 1 is almost symmetric and actually it has been mechanically designed to be physically symmetric.

The output of PAR2DOPT is shown in Fig. 2.2. The coordinates of the four corners of the insulated cable in the outer layer is given in Table 2.4 and in the inner layer in Table 2.5.

Table 2.4: Coordinates of the four corners of each conductor in the outer layer. The cable includes 6.6 mil radial insulation and 3.45 mil azimuthal insulation on it.

Turn No.	x_1 inch	y_1 inch	x_2 inch	y_2 inch	x_3 inch	y_3 inch	x_4 inch	y_4 inch
1	1.4836	0.00400	1.483	0.053	1.957	0.061	1.957	0.004
2	1.4824	0.05270	1.481	0.101	1.954	0.118	1.956	0.061
3	1.4797	0.10130	1.478	0.150	1.951	0.175	1.953	0.118
4	1.4755	0.14980	1.472	0.198	1.945	0.231	1.948	0.175
4	1.4697	0.19820	1.466	0.247	1.938	0.288	1.942	0.231
6	1.4625	0.24650	1.458	0.295	1.929	0.344	1.934	0.287
7	1.4537	0.29450	1.448	0.343	1.918	0.400	1.925	0.344
8	1.4434	0.34230	1.437	0.391	1.906	0.456	1.914	0.400
9	1.4317	0.38980	1.424	0.438	1.892	0.512	1.901	0.455
10	1.4184	0.43700	1.410	0.485	1.877	0.567	1.886	0.511
11	1.4037	0.48380	1.395	0.532	1.860	0.622	1.870	0.566
12	1.3777	0.55300	1.358	0.597	1.788	0.796	1.811	0.744
13	1.3584	0.59770	1.338	0.642	1.764	0.848	1.788	0.796
14	1.3377	0.64180	1.316	0.685	1.739	0.899	1.764	0.848
15	1.3157	0.68520	1.293	0.729	1.713	0.949	1.739	0.898
16	1.2923	0.72790	1.269	0.771	1.685	0.998	1.712	0.948
17	1.2676	0.76990	1.244	0.812	1.655	1.047	1.683	0.998
18	1.2416	0.81110	1.217	0.853	1.624	1.095	1.653	1.046
19	1.2143	0.85150	1.189	0.893	1.592	1.142	1.621	1.093
20	1.1857	0.89100	1.160	0.932	1.558	1.188	1.589	1.140
21	1.1559	0.92970	1.129	0.970	1.523	1.233	1.554	1.186
22	1.1248	0.96750	1.097	1.008	1.487	1.277	1.519	1.230
23	1.0925	1.00440	1.064	1.044	1.449	1.321	1.482	1.274
24	1.0591	1.04030	1.030	1.080	1.410	1.363	1.444	1.317
25	1.0244	1.07520	0.995	1.114	1.370	1.404	1.404	1.358
26	0.9886	1.10910	0.959	1.147	1.328	1.443	1.363	1.399

0.04 and 0.05. This requirement on $b_8^{'}$ threw many designs out of running. However, the final design which satisfied all of above requirements was no worse in performance to those which did not.

In Table 2.6 we have given the desired and optimized values of field harmonics in prime units. Harmonics, higher than $b_{12}^{'}$, had an optimized value of < 0.001, as desired. In the row of desired harmonics, we have also listed the tolerances in them. *"In magnet"* harmonics takes into account the pole notch and a flat face in the iron at the midplane. These are the expected values of low field harmonics in this magnet (not including the contributions from persistent currents in the superconductor).

Table 2.6: Desired and Optimized values of *low field* harmonics in prime units. The harmonics *in magnet* take into account the pole notch and a flat face in the iron at the midplane. These harmonics are in the units of 10^{-4}

Values	$b_2^{'}$	$b_4^{'}$	$b_6^{'}$	$b_8^{'}$	$b_{10}^{'}$	$b_{12}^{'}$
Desired	-.28±.4	.01±.1	0±.05	±(.04to.05)	0±.05	0±.05
Optimized	-0.280	0.009	-0.004	0.044	0.014	-0.001
In magnet	0.000	-0.001	-0.004	0.044	0.014	-0.001

We have used the following definition for field harmonics

$$B_y + iB_x = B_0 \sum_{n=0}^{\infty} [b_n + ia_n] [cos\,(n\theta) + i\ \ sin\,(n\theta)] \left(\frac{r}{R_0}\right)^n ,$$

where B_0 is the field at the center of the magnet, B_x and B_y the components of field at (r,θ), R_0 the normalization radius, a_n the skew harmonics and b_n the normal. These harmonics are usually quoted in prime units ($b_n^{'}$ and $a_n^{'}$) when R_0 is chosen to be 1 cm and the harmonics are given in 10^{-4} units.

3. Iron Yoke Design

In section 3.1 we shall discuss the optimization of the iron yoke. The yoke is optimized to produce a minimum change in field harmonics (due to iron saturation) for the maximum achievable value of transfer function at 6.6 Tesla. We used computer codes POISSON, MDP and PE2D for this purpose. In section 3.2 we shall discuss the computer model of the final design and the results of field calculations for it with POISSON, in section 3.3 with MDP and in section 3.4 with PE2D. An iron packing factor of 97.5% has been used in these calculations.

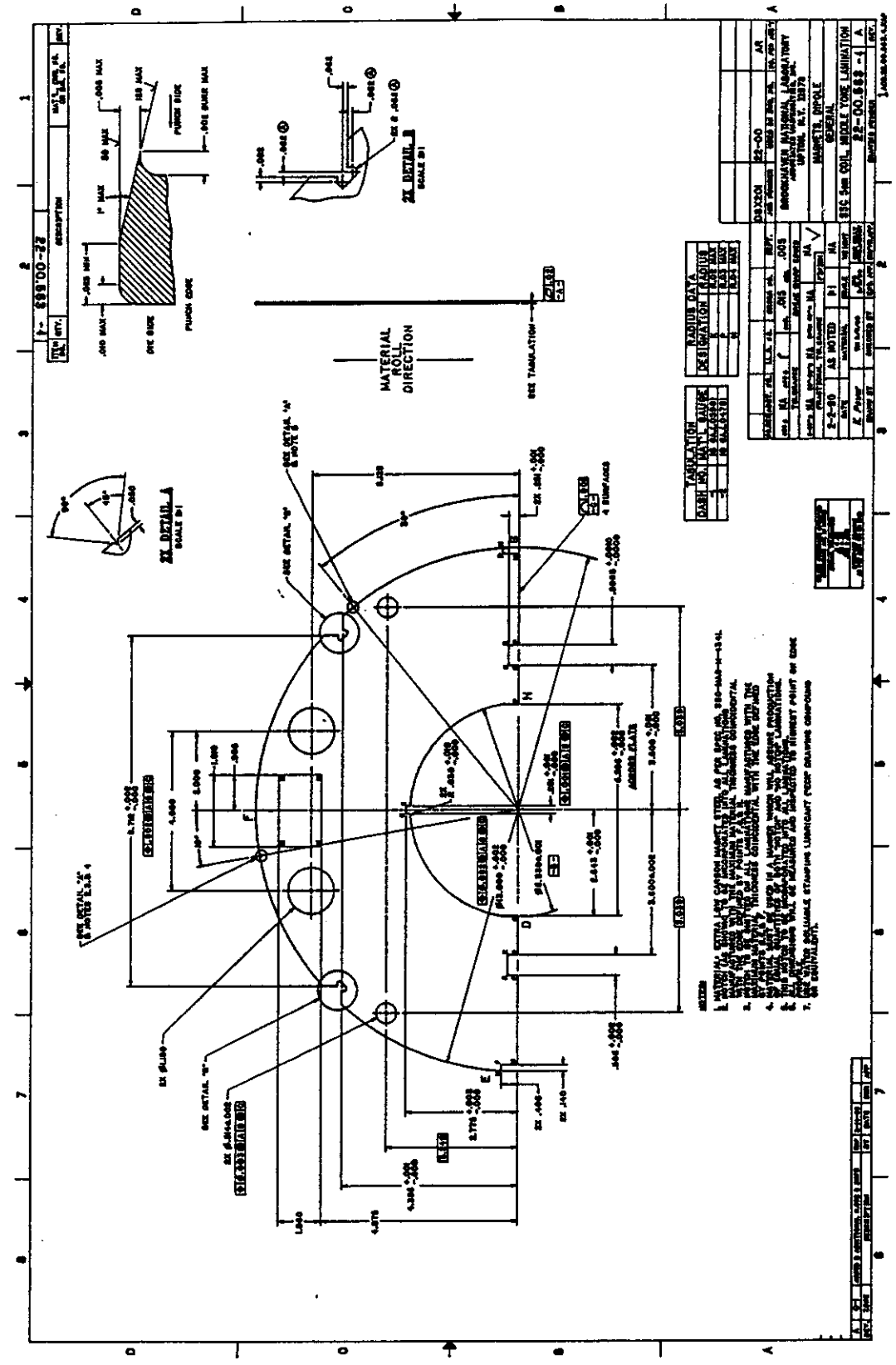

Figure 3.1: Optimized Yoke for DSX201/W6733

The values of the variables plotted in Fig. 3.2 is given in Table 3.1. The maximum b_2' saturation, as computed by POISSON, MDP and PE2D is about 0.3 prime unit. These three programs use three different methods for solving problem and it is encouraging to see that all predict a small saturation shift. The computed value of b_2' at 6.6 Tesla is about the same as it is at low field, which is zero.

Table 3.1: Transfer function and b_2' variation as function of current. In all cases b_2' is corrected to start from zero at 3.0 kAmp.

I	T.F. (T/kA)			$b_2' \times 10^{-4}$		
kAmp	POISSON	MDP	PE2D	POISSON	MDP	PE2D
3.0	1.0447	1.0430	1.0430	0.00	0.00	0.00
4.0	1.0441	1.0413	1.0423	0.09	0.05	0.12
5.0	1.0397	1.0364	1.0374	0.24	0.16	0.24
5.5	1.0340	1.0311	1.0319	0.27	0.21	0.36
6.0	1.0262	1.0236	1.0243	0.15	0.17	0.30
6.25	1.0219	1.0194	1.0201	0.08	0.11	0.19
6.5	1.0173	1.0148	1.0156	-0.02	0.03	0.21

In Table 3.2 we have listed the maximum change in b_2' and b_4' harmonics due to iron saturation. All other higher harmonics remain practically unchanged. In the same table we have also listed the drop in transfer function, $\delta(TF)$, till 6.6 Tesla as compared to its value at low field.

Table 3.2: Drop in transfer function till 6.6 Tesla and the maximum change in b_2' and b_4'; higher harmonics remain practically unchanged.

Harmonic	POISSON	MDP	PE2D
$\delta(TF)$, till 6.6T	2.62%	2.70%	2.63 %
$\delta(b_2')_{max}$, 10^{-4}	0.28	0.22	0.36
$\delta(b_4')_{max}$, 10^{-4}	-0.03	-0.02	-0.04

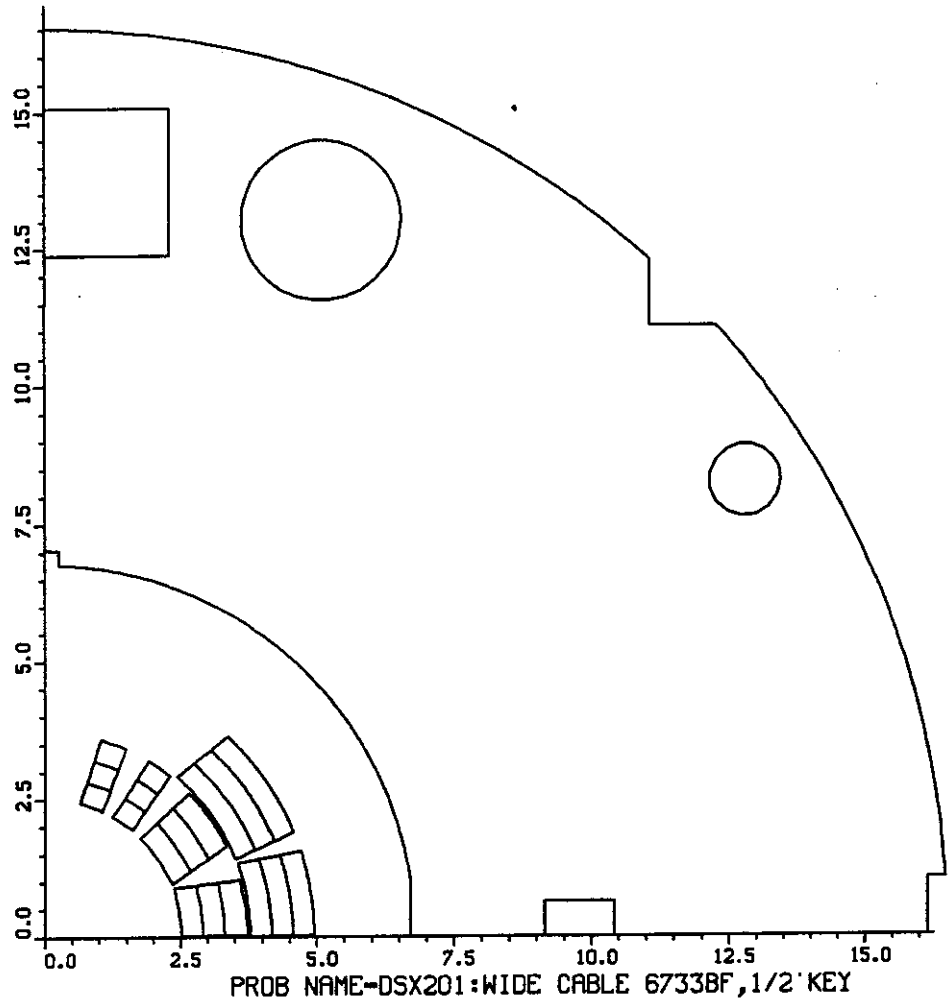

Figure 3.3: POISSON model for DSX201/W6733.

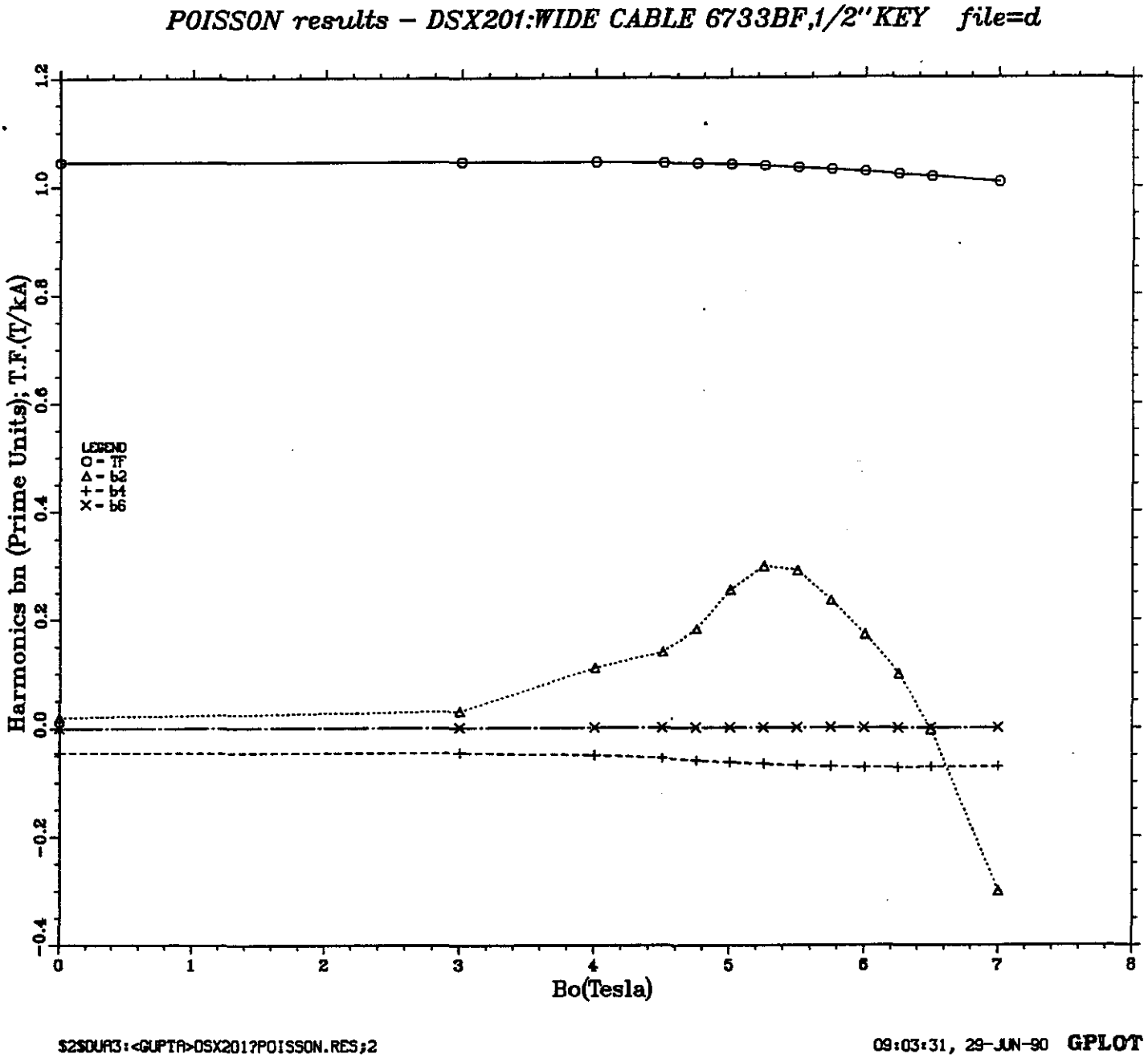

Figure 3.5: Variation in Field Harmonics as a function of B_o for DSX201 as computed by POISSON.

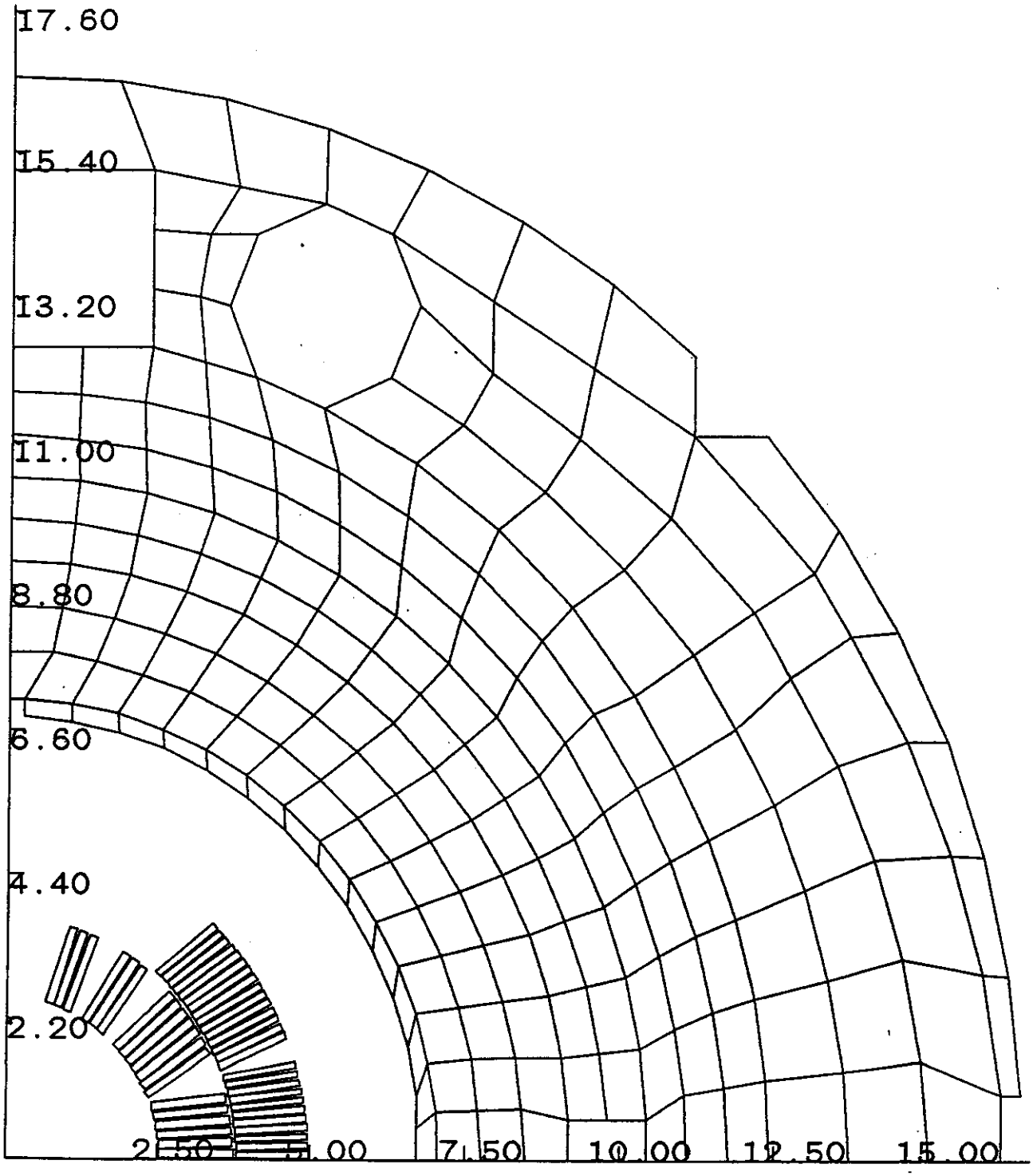

Figure 3.6: MDP model for DSX201/W6733.

3.4 PE2D Calculations

The computer code PE2D solves for the vector potential using a finite element method. The computer model of DSX201/W6733 on PE2D is shown in Fig. 3.8. In Table 3.5 we present the results of field calculations for various values of current in each turn. In Fig. 3.9, we plot the variation of field harmonics as a function of central field.

Table 3.5: Results of PE2D computations for DSX201/W6733.

I kAmp	B_o Tesla	T.F. T/kA	b_2' 10^{-4}	b_4' 10^{-4}	b_6' 10^{-4}	b_8' 10^{-4}	b_{10}' 10^{-4}
1.000	1.0431	1.04309	0.886	0.069	0.039	0.035	0.016
3.000	3.1289	1.04298	0.889	0.071	0.036	0.035	0.016
4.000	4.1690	1.04226	1.011	0.065	0.035	0.035	0.016
4.500	4.6832	1.04071	1.055	0.053	0.035	0.035	0.016
4.750	4.9366	1.03929	1.043	0.049	0.034	0.035	0.016
5.000	5.1870	1.03740	1.128	0.056	0.034	0.035	0.016
5.500	5.6753	1.03187	1.245	0.034	0.029	0.033	0.016
5.750	5.9119	1.02816	1.147	0.027	0.031	0.035	0.016
6.000	6.1457	1.02428	1.190	0.039	0.030	0.035	0.016
6.250	6.3757	1.02011	1.077	0.017	0.033	0.038	0.017
6.500	6.6016	1.01563	1.103	0.058	0.039	0.037	0.017
7.000	7.0462	1.00660	1.018	0.079	0.040	0.037	0.017

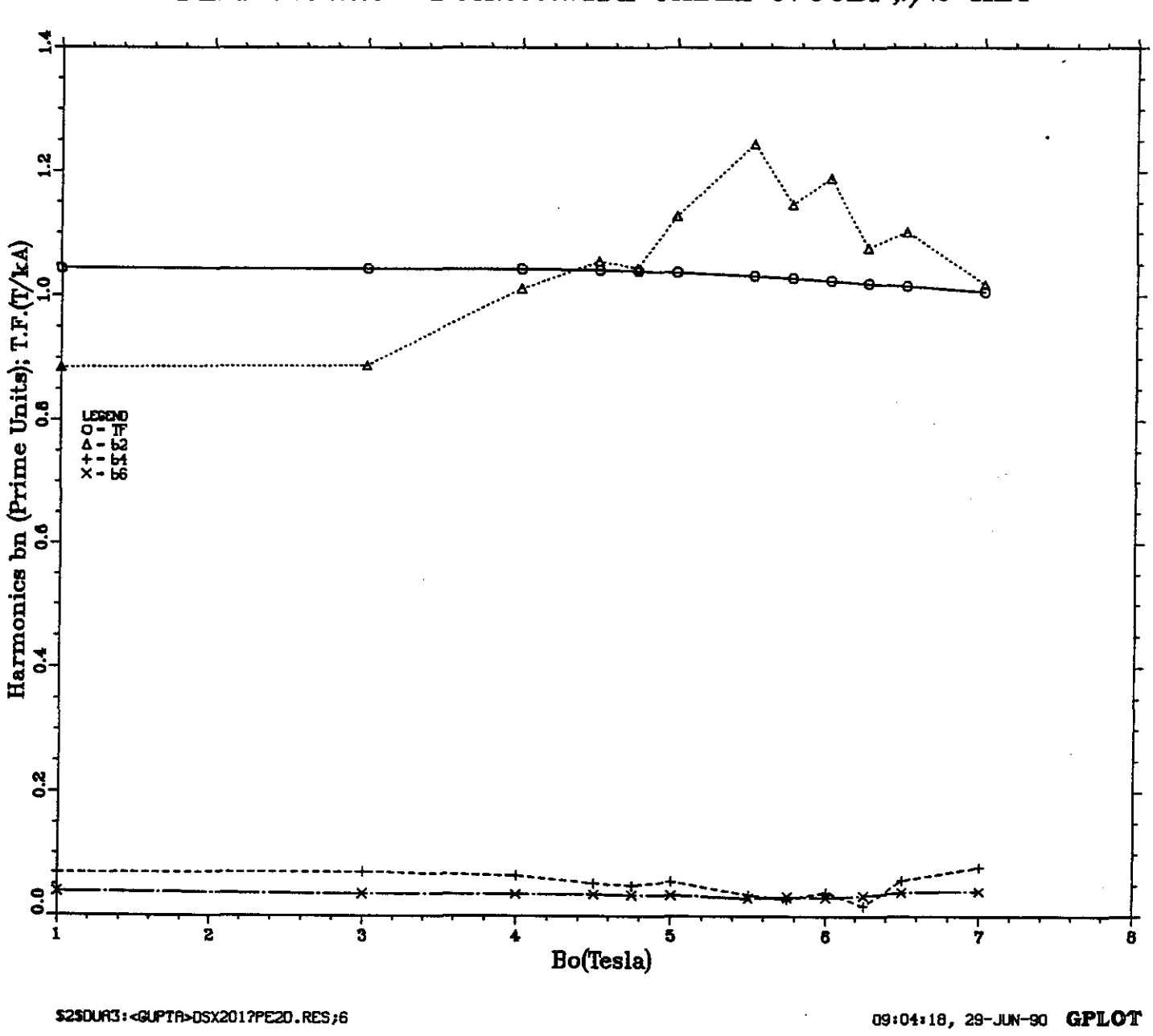

Figure 3.9: Variation in Field Harmonics as a function of B_o for DSX201/W6733 as computed by PE2D.

Table 4.2: Expected quench performance of DSX201/W6733 with 5% cable degradation ($J_c = 2612.5 Amps/mm^2$) and at 4.35° Kelvin bath temperature.

Layer ↓	Cu/Sc Ratio	B_{ss} Tesla	I_c Amp	B_{margin} %	T_{margin} Kelvin	S_{quench} Amp/cm^2	$S_{6.6T}$ Amp/cm^2
Inner	1.7	7.149	7126	8.3	0.519	736	671
	1.5	7.273	7273	10.2	0.625	788	704
	1.3	**7.399**	**7411**	**12.1**	**0.730**	**853**	**748**
Outer	2.0	7.268	7267	10.1	0.580	919	822
	1.8	**7.445**	**7470**	**12.8**	**0.709**	**980**	**852**

Table 4.3: Expected quench performance of DSX201/W6733 with 5% cable degradation ($J_c = 2612.5 Amps/mm^2$) and at 4.0° Kelvin bath temperature.

Layer ↓	Cu/Sc Ratio	B_{ss} Tesla	I_c Amp	B_{margin} %	T_{margin} Kelvin	S_{quench} Amp/cm^2	$S_{6.6T}$ Amp/cm^2
Inner	1.7	7.455	7481	13.0	0.869	773	671
	1.5	7.571	7615	14.7	0.975	826	704
	1.3	~ 7.654	~ 7711	~16.0	~1.080	~ 888	~748
Outer	2.0	7.642	7697	15.8	0.930	973	822
	1.8	7.825	7908	18.6	1.059	1037	852

Table 4.4: Expected quench performance of DSX201/W6733 with 10% cable degradation ($J_c = 2475.0 Amps/mm^2$) and at 4.35° Kelvin bath temperature.

Layer ↓	Cu/Sc Ratio	B_{ss} Tesla	I_c Amp	B_{margin} %	T_{margin} Kelvin	S_{quench} Amp/cm^2	$S_{6.6T}$ Amp/cm^2
Inner	1.7	7.058	7023	6.9	0.439	726	671
	1.5	7.186	7169	8.9	0.552	777	704
	1.3	7.318	7319	10.9	0.663	842	748
Outer	2.0	7.129	7106	8.0	0.472	899	822
	1.8	7.307	7311	10.7	0.609	959	852

Fig. 3.4. Next we estimate the effect of changing the wedge size by +2 mil. Pole angle is held constant in this calculation by reducing the conductor thickness by an appropriate amount. The counting scheme for the wedges is the same as it was for the current blocks. We also estimate the effect of increasing the pole angle by 2 mil in the inner and in the outer layer. We compute the Root Mean Square (RMS) change for these groups of variations and in the end we compute the total RMS change produced by all of above variations combined.

Table 5.1: The effect of 2 mil change in the given parameter on the Transfer Function, Field harmonics and χ^2.

Parameter changed	TF T/kA	b_2' 10^{-4}	b_4' 10^{-4}	b_6' 10^{-4}	χ^2 10^{-7}
Block No. 1	0.30	-0.25	-0.10	-0.01	0.10
Block No. 2	-0.31	0.31	0.11	0.01	0.15
Block No. 3	-0.13	0.35	-0.02	-0.01	0.13
Block No. 4	-0.20	0.32	-0.08	0.01	0.13
Block No. 5	-0.10	-0.04	-0.01	0.00	0.00
Block No. 6	-0.79	0.23	0.03	0.00	0.06
RMS Blocks	0.38	0.27	0.07	0.01	0.11
Wedge No. 1	6.99	-0.57	0.03	0.01	0.33
Wedge No. 2	9.36	0.48	0.05	-0.01	0.24
Wedge No. 3	10.83	0.59	-0.04	0.00	0.36
Wedge No. 4	9.75	-0.01	0.00	0.00	0.00
RMS Wedges	9.34	0.48	0.04	0.01	0.27
Pole angle inner	-12.47	-0.34	0.05	-0.01	0.13
Pole angle outer	-12.54	-0.52	0.00	0.00	0.27
RMS Pole angles	12.51	0.44	0.04	0.01	0.21
Total RMS	7.43	0.38	0.06	0.01	0.19

Table 6.2: Lorentz Force Calculations for the turns in the outer layer

Turn No.	X_c cm	Y_c cm	B_x Tesla	B_y Tesla	F_r Lbs/in	F_θ Lbs/in
20	4.369	0.077	-0.050	-0.355	13.1	-2.1
21	4.365	0.211	-0.229	-0.366	13.2	-9.2
22	4.357	0.345	-0.408	-0.389	13.2	-16.2
23	4.344	0.479	-0.585	-0.423	13.2	-23.3
24	4.328	0.612	-0.761	-0.468	13.3	-30.4
25	4.307	0.745	-0.937	-0.525	13.3	-37.6
26	4.283	0.877	-1.113	-0.591	13.2	-44.9
27	4.255	1.009	-1.290	-0.665	13.0	-52.3
28	4.222	1.140	-1.471	-0.744	12.4	-59.9
29	4.186	1.270	-1.659	-0.822	11.3	-67.8
30	4.146	1.399	-1.856	-0.894	9.4	-75.9
31	4.022	1.708	-1.350	-0.889	10.8	-59.0
32	3.968	1.831	-1.524	-1.043	11.5	-67.6
33	3.910	1.952	-1.694	-1.191	11.5	-76.0
34	3.848	2.071	-1.859	-1.339	11.1	-84.3
35	3.783	2.188	-2.020	-1.492	10.4	-92.6
36	3.714	2.303	-2.177	-1.656	9.7	-101.1
37	3.642	2.416	-2.330	-1.833	8.9	-109.7
38	3.567	2.527	-2.478	-2.025	8.2	-118.5
39	3.488	2.636	-2.623	-2.233	7.4	-127.6
40	3.405	2.743	-2.765	-2.459	6.7	-137.2
41	3.320	2.847	-2.907	-2.703	5.9	-147.2
42	3.231	2.948	-3.053	-2.969	5.0	-158.0
43	3.139	3.047	-3.207	-3.257	3.8	-169.6
44	3.044	3.144	-3.380	-3.570	2.0	-182.4
45	2.946	3.238	-3.579	-3.909	-0.6	-196.7
45	2.946	3.238	-3.579	-3.909	-0.6	-196.7

TECHNICAL NOTE DISTRIBUTION

Building 902

Blake, A.
Cottingham, J. G.
Garber, M.
Ghosh, A.
Greene, A.
Gupta, R.
Herrera, J.
Kahn, S.
Kelly, E.
Morgan, G.
Muratore, J.
Prodell, A.
Rehak, M.
Rohrer, E.P.
Sampson, W.
Shutt, R.
Thompson, P.
Wanderer, P.
Willen, E.

Building 1005S

Brown, D.
Claus, J.
Courant, E.
Dell, F.
Flood, A.
Lee, S.Y.
Mulutinovic, J.
Ozaki, S.
Parzen, G.
Rhoades-Brown, M.
Ruggiero, S.
Sondericker, J.
Tepekian, S.
Wolff, L.

Building 911

AD Library, (H. Martin)
P. Hughes (1) plus one for ea. author
Mangra, D.

Building 460

Samios, N. P.

For SSC Papers

FNAL
Bossert, R.
Carson, J.
Mantsch, P.
Markley, F.
Strait, J.
Koska, W.

SSCL

Bush, T.
Capone, D.
Coombes, R.
Devred, A.
Harley,
Haddock, C.
Kozman, T.
Lloyd,
Orrell. D.
Palmer, R.
Pewitt, D.
Sanger, P.
Snitchler, G.
Sudtelgte, B.
Tompkins, J.
Zbasnik, J.

LBL
Caspi, S.
Dell'Orco, D.
Taylor, C.

S&P in Magnet Division for all MD papers

S&P in Accelerator Physics Division for all Cryogenic Papers (and J. Briggs, R. Dagradi, H. Hildebrand, W. Kollmer